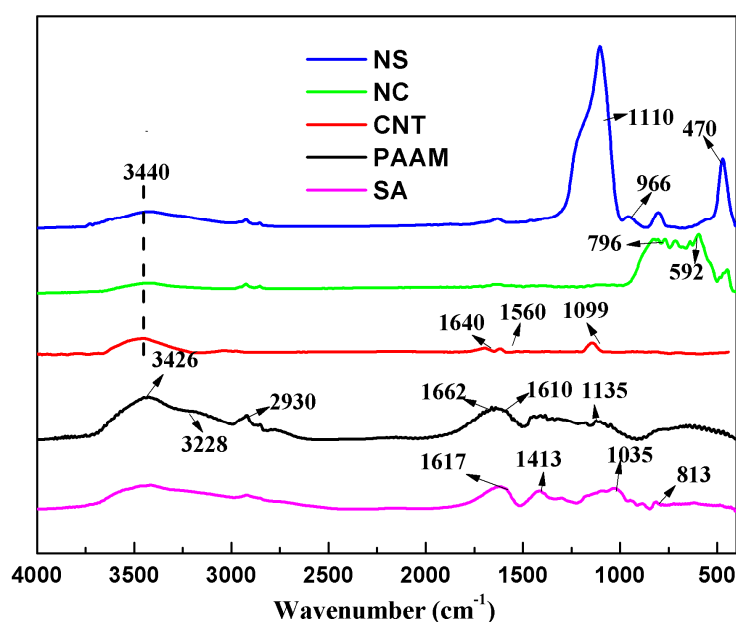


## 1. Chemical structure of PAAM, SA, CNT, NC and NS

For better understanding the FTIR results, the spectra of PAAM, SA, CNT, NC and NS present in Figure S1. It can be seen that the absorption peaks at  $3440\text{ cm}^{-1}$  which were attributed to the stretching of  $-\text{OH}$  was shown in all the spectra, suggesting the presence of hydroxyl groups on the surface of three inorganic nanoparticles. The IR spectrum of PAAM exhibited characteristic peaks at  $3426$  and  $3228\text{ cm}^{-1}$ , representing asymmetric and symmetric  $\text{N-H}$  stretching vibrations [1]. The peaks at  $1135\text{ cm}^{-1}$  implied the  $\text{C-N}$  and  $\text{N-H}$  at  $\text{CONH}_2$  group [2] and the bands at  $1662$ ,  $1610$  and  $2930\text{ cm}^{-1}$  assigned to  $\text{CO}$  stretching,  $\text{NH}$  bending,  $\text{CH}$  stretching, respectively. In the spectrum of SA, two bands at  $1617$  and  $1413\text{ cm}^{-1}$  corresponded to  $\text{COO}^-$  group and one sharp peak at  $1035\text{ cm}^{-1}$  were responsible for  $\text{C-O}$  vibration. Moreover, the characteristic peak appeared at  $813\text{ cm}^{-1}$  on SA depicted the  $\text{Na-O}$  vibration [3]. Due to the vibration of the carbon skeleton, the spectrum of CNT showed a characteristic band at  $1560\text{ cm}^{-1}$  [4]. The absorption peaks at  $1640\text{ cm}^{-1}$  and  $1099\text{ cm}^{-1}$  may originate to  $\text{O-H}$  vibrations of adsorbed water and  $\text{C-O-C}$  bending on CNT [5]. For IR spectrum of NC, the absorption bands in the range of  $838\text{ cm}^{-1}$ - $450\text{ cm}^{-1}$  were attributed to  $-\text{OH}$  bending and  $\text{M-O}$  ( $\text{M}$  denotes  $\text{Si}$  or other metal cations existed in clay) [6]. Particularly, the two peaks at  $796$  and  $592\text{ cm}^{-1}$  of NC were ascribed to the deformation vibration of  $\text{Al-O-Si}$  bonds [7]. The analyzing of NS spectrum was specified in the manuscript.



**Figure S1.** FTIR spectra of PAAM, SA, CNT, NC and NS.

## 2. The effects of pH and adsorbent dosage on adsorption

The adsorption experiments were carried out by using  $120\text{ mg}$  prepared hydrogels in  $150\text{ ml}$  of  $\text{Cu}^{2+}$  solution at  $25^\circ\text{C}$ . For investigating the effect of pH on adsorption, the concentration of  $\text{Cu}^{2+}$  was selected as  $150\text{ mg/L}$ . For inquiring the effect of hydrogel dosages on adsorption, various  $\text{Cu}^{2+}$  concentrations ( $20$ - $120\text{ mg/L}$ ) were applied to the experiments. After reaching adsorbent equilibrium, the adsorbents were removed from the solution. The concentrations of  $\text{Cu}^{2+}$  were determined by Flame Atomic Absorption Spectrometer (FAAS, TAS-990, Persee,

Beijing, China).

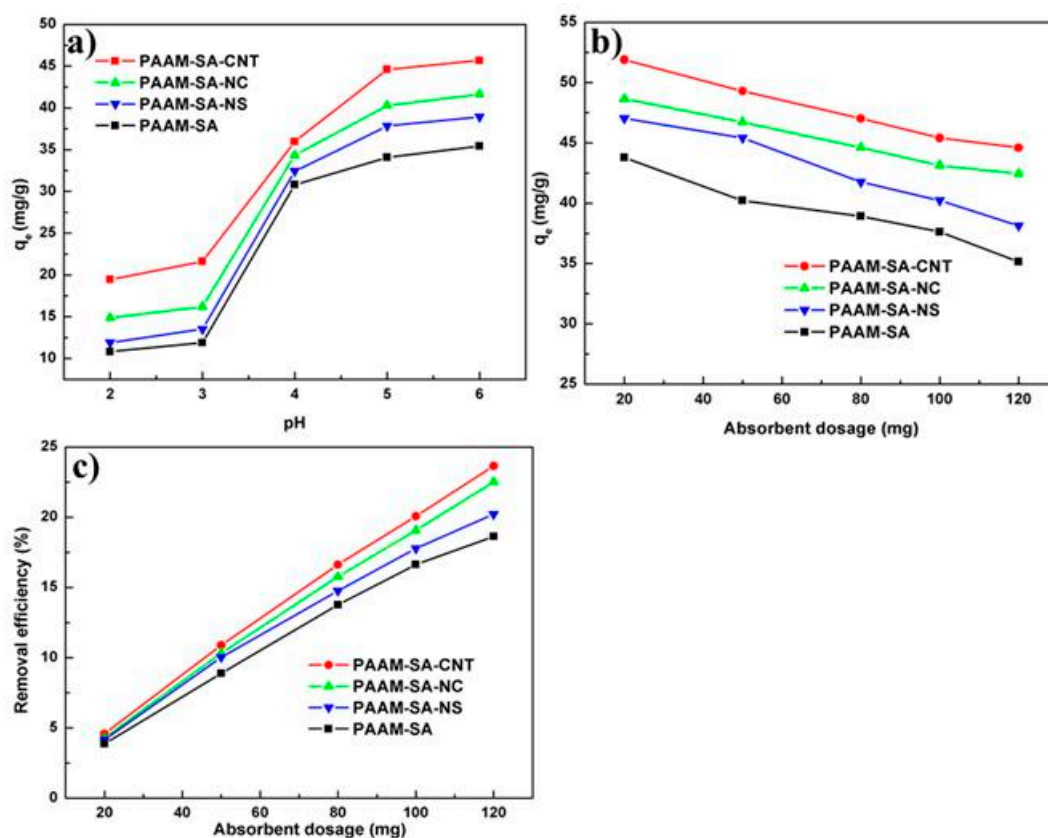


**Figure S2.** The adsorption of Cu<sup>2+</sup> on hydrogels: (a) the effects of pH; (b) the adsorbent dosages versus the adsorption capacities at equilibrium; (c) the adsorbent dosages versus removal efficiencies.

Figure S2a displays the adsorption capacities of the hydrogels to Cu<sup>2+</sup> at pH ranging from 2 to 6. In this study, pH above 6.0 was not studied because the Cu(OH)<sub>2</sub> would be produced at pH higher than 6.0. At pH ranging of 2-6, the adsorption abilities of the hydrogels were gradually increased with the increasing of pH. The adsorption rates were low at pH level of 2-3. The possible reason was that the -NH<sub>2</sub> groups in the PAAM chains were protonated resulting in a positively surface charge of the hydrogels. Hence, the electrostatic repulsion between positively charged hydrogel surface and positively charged Cu<sup>2+</sup> inhibited the adsorption of Cu<sup>2+</sup> on hydrogels. In addition, there were more H<sup>+</sup> at lower pH levels and these H<sup>+</sup> could compete with Cu<sup>2+</sup> for the adsorption site, which also led to a decrease in adsorption capacity [8]. With the increasing of pH values, -NH<sub>2</sub> groups were not ionized whereas -COOH and -OH groups were ionized. The negatively charged -COO<sup>-</sup> and -O<sup>-</sup> groups improved the adsorption by electrostatic interactions with Cu<sup>2+</sup> [9]. The obtained results are in accordance with previous literatures [8-10]. The effects of the amounts of adsorbent on the adsorption of Cu<sup>2+</sup> are showed in Figure S2b and S2c. The adsorption capacities decreased with the increasing of the sorbent dosage from 20 to 120mg, however, the total removal efficiencies of Cu<sup>2+</sup> gradually increased. This phenomenon was attributed to the number of active groups on the surface of the hydrogel increased for adsorbing Cu<sup>2+</sup> [10, 11].

## References

1. Gad, Y.H.; Aly, R.O., and Abdel-Aal, S.E., Synthesis and characterization of Na-alginate/acrylamide hydrogel and its application in dye removal. *Journal of Applied Polymer Science*, **2011**, *120*, 1899–1906.
2. Al-Kahtani, A.A. and Sherigara, B.S., Semi-interpenetrating network of acrylamide-grafted-sodium alginate microspheres for controlled release of diclofenac sodium, preparation and characterization. *Colloids and Surfaces B-Biointerfaces*, **2014**, *115*, 132–138.
3. Li, P.; Yan, L.; Huang, J.; Li, J.; Gong, J., and Ma, J., Microfluidic Fabrication of Highly Stretchable and Fast Electro-responsive Graphene Oxide/Polyacrylamide/Alginate Hydrogel Fibers. *European Polymer Journal*, **2018**, *103*, 335–341.
4. Poernomo, G.; Cong, G.; Xianghua, S.; Quanyuan, Z.; Leong, S.S.J.; Chuyang, T.; Yuan, C.; Chan-Park, M.B.; Matthew Wook, C. and Kean, W., Hollow fiber membrane decorated with Ag/MWNTs: toward effective water disinfection and biofouling control. *ACS Nano*, **2011**, *5*, 10033–10040.
5. Han, J.; Wang, H.; Yue, Y.; Mei, C.; Chen, J.; Huang, C.; Wu, Q. and Xu, X., A self-healable and highly flexible supercapacitor integrated by dynamically cross-linked electro-conductive hydrogels based on nanocellulose-templated carbon nanotubes embedded in a viscoelastic polymer network. *Carbon*, **2019**, *149*, 1–18.
6. Zhang, J. and Wang, A., Study on superabsorbent composites. IX: Synthesis, characterization and swelling behaviors of polyacrylamide/clay composites based on various clays. *Reactive and Functional Polymers*, **2007**, *67*, 737–745.
7. Mao, X.; Wang, L.; Gu, S.; Duan, Y.; Zhu, Y.; Wang, C., and Lichtfouse, E., Synthesis of a three-dimensional network sodium alginate-poly(acrylic acid)/attapulgit hydrogel with good mechanic property and reusability for efficient adsorption of Cu<sup>2+</sup> and Pb<sup>2+</sup>. *Environmental Chemistry Letters*, **2018**, 1–6.
8. Tong, D.; Fang, K.; Yang, H.; Wang, J.; Zhou, C., and Yu, W., Efficient removal of copper ions using a hydrogel bead triggered by the cationic hectorite clay and anionic sodium alginate. *Environmental Science and Pollution Research*, **2019**, *26*, 16482–16492.
9. Wang, M.; Li, X.; Zhang, T.; Deng, L.; Li, P.; Wang, X., and Hsiao, B.S., Eco-friendly poly(acrylic acid)-sodium alginate nanofibrous hydrogel: A multifunctional platform for superior removal of Cu(II) and sustainable catalytic applications. *Colloids and Surfaces A-Physicochemical and Engineering Aspects*, **2018**, *558*, 228–241.
10. Milosavljevic, N.; Debeljkovic, A.; Krusic, M.K.; Milasinovic, N.; Uzum, O.B., and Karadag, E., Application of Poly(acrylamide-co-sodium methacrylate) Hydrogels in Copper and Cadmium Removal from Aqueous Solution. *Environmental Progress and Sustainable Energy*, **2014**, *33*, 824–834.
11. Zou, X.; Zhang, H.; Chen, T.; Li, H.; Meng, C.; Xia, Y., and Guo, J., Preparation and characterization of polyacrylamide/sodium alginate microspheres and its adsorption of MB dye. *Colloids and Surfaces A: Physicochemical and Engineering Aspects*, **2019**, *567*, 184–192.